

pubs.acs.org/Macromolecules Article

Influence of Membrane Permittivity on Charge Regulation of Weak Polyelectrolytes End-Tethered in Nanopores

Shiyi Qin, Rikkert J. Nap, Kai Huang, and Igal Szleifer*



Cite This: Macromolecules 2022, 55, 8384-8398



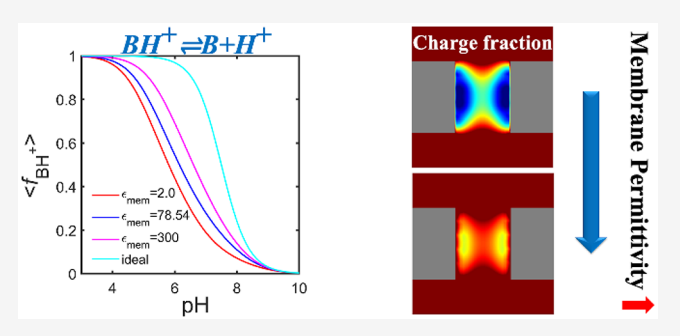
ACCESS I

III Metrics & More

Article Recommendations

Supporting Information

ABSTRACT: Artificial nanopores functionalized with weak polyelectrolytes are an interesting and important class of stimuli-responsive nanofluidic devices. So far, the effects of the dielectric properties of the supporting nanopore surface on the behavior of the nanopore are largely unexplored. Here, we theoretically investigate the influence that the dielectric mismatch between solvent and nanopore surface has on the charge regulation of weak polyelectrolyte brushes inside the nanopore. Our approach is based on a molecular theory that explicitly incorporates the coupling between molecular organization, physical interactions, and chemical equilibrium. It is further extended to consider both the



dielectric properties of the supporting surface of the nanopore as well as those of the nanopore solvent and polymer layer. We find that the surface polarization plays a crucial role in modulating the charge and structure of the weak polyelectrolytes that are end-tethered to the inner wall of the nanopore. Likewise, the surface polarization influences the nanoscale transport through the nanopore. We demonstrate that different dielectric properties of the nanopore membrane can result in large changes in the local ion distribution and electrostatic potential around the ionizable groups of the weak polyelectrolytes, which simultaneously alter the charge and structure of the polyelectrolyte layer inside the nanopore. Our quantitative approach systematically reveals how various intrinsic and external factors such as bulk salt concentration, polymer grafting density, and polymer length influence the surface polarization and its effects on properties such as the charge of the polyelectrolyte layer. For specific conditions, we report a high sensitivity of translocating cargoes to the changes in the dielectric properties of the polyelectrolyte-coated nanopore surface.

■ INTRODUCTION

End-grafted polyelectrolytes, also known as polyelectrolyte brushes, have become a versatile way to fabricate functionalized interfaces with externally programmable characteristics ^{1–4} and have been extensively used in a wide range of applications such as colloidal stabilization ^{5–7} and surface lubrication. ^{8–10} They have been the focus of both theoretical and experimental research to understand their unique properties and potential applications.

Recent advancements in manufacturing and polymer synthesis techniques have made it possible to graft polymer chains to the inner walls of artificial nanopores. The use of responsive and switchable polymers allows the functionalized nanochannel to alter its structural morphology in response to external environmental changes and cues. Their morphological changes can be utilized to, for example, control the conduction and endow the nanopore with gating abilities. The possibility of incorporating responsive functions into confined geometries represents a significant step forward in the development of smart nanochannel systems. As a representative example, weak polyelectrolytes have been widely integrated into the nanopores to create a pH-responsive transport system. The nanoconfined environments inside nanopores greatly enhance the coupling between physical

interactions, chemical equilibrium, and molecular organization. As a result, the behavior of polymers under nanoconfinement can be very different from that in solution. For endtethered weak polyelectrolytes in nanopores, a shift of acid—base equilibrium compared to that of the same polymer in a dilute solution occurs. Changes in charge are also accompanied by variations in the electrostatic interaction and polymer structure.

With the high demand for nanopores in a variety of applications, a wide spectrum of materials, including both low^{31,32} and high^{33–36} dielectric materials, are being proposed as substrates in synthetic devices. The substrate permittivity is another variable that affects the properties of polyelectrolytes inside nanopores. The dielectric mismatch between the solvent and the nanopore surface induces surface polarization charges that will alter the electrostatic interactions within the pore, and

Received: July 5, 2022 Revised: August 30, 2022 Published: September 13, 2022





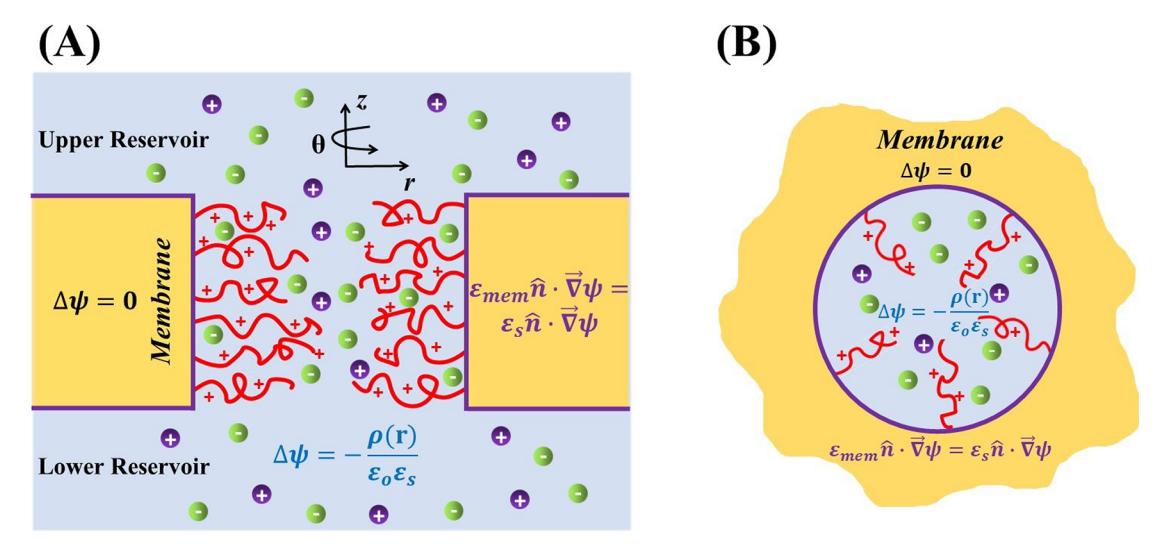


Figure 1. Schematic representation of the nanopore: (A) side view and (B) top view. The cylindrical nanopore has radius *R* in a membrane of thickness *L*. The membrane connects two identical reservoirs containing salt anions and cations as well as protons and hydroxyl ions. The inner wall of the pore is modified with weak polybase chains. The governing equations for the electric potential inside and outside the membrane as well as the boundary conditions at the membrane interface are listed in the figure.

this can affect the charge regulation of the weak polyelectrolytes when anchored to the pore's substrate. Moreover, prior theoretical research for bare nanopores functionalized with surface moieties that carry fixed charges demonstrated that the polarization effect influences the properties of the nanopores.^{37,38} Taken all together, this suggests that polarization effects have the potential to modulate the electrostatic environment and impact the charge regulation process of weak polyelectrolytes under nanoconfinement. So far, the effect of substrate permittivity on the properties of nanopores functionalized with charge regulating polyelectrolytes has not received much attention yet, both experimentally and theoretically. This is mainly due to the difficulty of experimental visualization of nanoconfined spaces and a lack of simulation techniques that can integrate polymer conformations, chemical reactions, and dielectric boundary conditions. Only recently, Luijten and co-workers³⁹ using molecular dynamics (MD) demonstrated the effect that surface polarization has on the ion distribution near a strong polyelectrolyte brush grafted to the planar surface. Strong polyelectrolytes have fixed charges, opposite to weak polyelectrolytes, whose degree of ionization is variable and depends on pH, salt concentration, and polymer density. An enhanced concentration of counterions near high-permittivity substrates is observed whereas the opposite situation happens near low-permittivity surfaces. Dielectric modulation of polyelectrolyte structures has later been investigated in the system of a planar strong polyelectrolyte brush 40 and a strong polyelectrolyte confined in a spherical cavity. 41 Lujiten et al. also applied MD simulations to study surface-functionalized nanoparticles and investigated the combined effect that surface polarization and charge regulation of chemical surface moieties have on the self-assembly of these nanoparticles. 42 So far, efforts to understand the impact of dielectric surface properties on the behavior of polyelectrolytes, tethered or free, have focused on strong polyelectrolytes. The influence of surface dielectric on weak (tethered) polyelectrolytes has not been studied, as far as we are aware. However, the recent findings for strong polyelectrolyte systems suggest that dielectric mismatch will affect the properties of surface-tethered weak polyelectrolytes inside the nanopore. Because of the pH-responsive nature of weak polyelectrolytes, we anticipated a stronger and more complicated effect of dielectric mismatch. Hence, here we investigated how the relative permittivity of the pore membrane will influence and control the properties of weak polyelectrolytes end-grafted to the inner surface of the nanopore.

We employ a molecular theory to study the effect of the dielectric properties of a nanopore surface on the charge regulation of weak polyelectrolytes confined in the nanopore. This molecular theory has been proven to be powerful in quantitatively predicting the structural and thermodynamical properties of various systems involving end-tethered polymer layers. 26,27,29,43-45 Theoretical predictions from our theory were shown to be in good agreement with the experimental observations. 29,46-48 For example, the ionic conductance of a nanochannel functionalized with weak polybases predicted from the molecular theory was found to agree well with experimental measurements.²⁹ The predictive power of the molecular theory gives us confidence in its ability to properly represent the behavior of polymer-grafted nanopores and to accurately characterize relevant properties such as polymer charge and structure.

In our previous studies of functionalized nanopores and nanochannels, it had been assumed that the membrane consisted of a low-dielectric material whose dielectric constant can effectively be considered to be zero ($\varepsilon_{\rm mem}=0$). 26,28,29 For $\varepsilon_{\rm mem}=0$, the electric (displacement) field inside the membrane is zero by construction, and we do not explicitly need to consider the electric field inside the membrane. Here we extended the theoretical approach and included the electrostatic interaction of the membrane by explicitly solving the electrostatic governing equation inside the membrane as well. This allows us to investigate nanopores with membranes that have different (nonzero) dielectric constants.

A schematic of the nanopore studied here is shown in Figure 1. The nanopore is functionalized by end-grafting weak polyelectrolytes to the inner wall of the pore. The polyelectrolytes are composed of basic monomers, and the pK_s is set to be 7.5, which corresponds to a weak polybase such

as poly(2-(dimethylamino)ethyl methacrylate) (PDMEA-MA).⁴⁹ On the basis of the relative dielectric constant of the inner pore wall, we can separate three different dielectric constant regimes, namely (i) the low $\varepsilon_{\mathrm{mem}}$ regime, where $\varepsilon_{\mathrm{mem}}$ < $\varepsilon_{\rm s}$ ($\varepsilon_{\rm s}$, the dielectric constant of the solution, is set as 78.54 to represent water); (ii) the intermediate ε_{mem} regime, where $\varepsilon_{\rm mem} = \varepsilon_{\rm s}$; and (iii) the high $\varepsilon_{\rm mem}$ regime, where $\varepsilon_{\rm mem} > \varepsilon_{\rm s}$. We investigated representative cases for each of the different regimes. More specifically, we considered $\varepsilon_{\rm mem}$ equal to 0, 2, 78.54, and 300. $\varepsilon_{\rm mem}$ = 2 corresponds to the relative dielectric constant of a lipid membrane. Other examples of low dielectric constant materials are quartz and mica. 31,32,51-53 The case of $\varepsilon_{\text{mem}} = 0$ is also included here to compare with the membrane that has a dielectric constant of ε_{mem} = 2. We compare both cases to verify and validate our previous approximation of zero dielectric constant for low-permittivity nanopore membranes. Oppositely, materials, such as titanium dioxide and strontium titanate, can be considered to have a "high" dielectric constant, as compared to water, and have a dielectric constant in the range $150-300.^{34-36,54}$ We also studied the membrane with $\varepsilon_{\rm mem}$ = 78.54, which reflects the absence of any dielectric mismatch between the inner pore wall and the solution.

We found that the dielectric properties of the membrane, depending on environmental conditions such as pH and salt concentration, can have a large effect on the charging behavior of weak polyelectrolytes inside the nanopore. When the nanopore membrane has a low dielectric constant, $\varepsilon_{\rm mem} < \varepsilon_{\rm s}$ the shift of acid-base equilibrium toward neutral state is even more significant compared to a pore wall that has no dielectric mismatch with its aqueous polymer solution region, $\varepsilon_{\rm mem} = \varepsilon_{\rm s}$ while a relatively smaller shift in the chemical equilibrium is observed for a nanopore whose membrane has a high dielectric constant, $\varepsilon_{\rm mem} > \varepsilon_{\rm s}$. We also observe morphological changes in the polyelectrolyte brush. The observed changes stem from the fact that the permittivity mismatch at the solvent-membrane interface gives rise to a surface polarization, which provides additional electrostatic interactions between the nanopore surface and the charged polyelectrolytes. The translocation of a nanoparticle through the nanopore is also investigated to illustrate how the structural changes induced by different dielectric membrane properties affect the transport performance of large cargoes. Moreover, we systematically show that the influence of dielectric mismatch on charge regulation of polyelectrolytes can be controlled by varying different system conditions such as bulk salt concentration, polymer grafting density, and polymer length. The insights from this work deepen our understanding of the role dielectric surface properties play in the charge regulation of end-tethered polyelectrolytes and guide the rational design of bioinspired nanodevices.

■ THEORETICAL METHODS

The theoretical framework in this work is based on a previously developed molecular theory ^{26,29,44,55,56} that explicitly incorporates the molecular details of the system such as the size, shape, charge distribution, and conformations of all molecular species in the system. It also takes into account the relevant intramolecular and intermolecular interactions as well as the chemical equilibrium of the basic monomers. To model the structural and thermodynamic properties of the current system, we extended the theory by considering the dielectric mismatch between the solvent and the membrane. The free

energy functional that describes a nanopore modified with endtethered weak polyelectrolytes has several distinct contributions, which can be summarized as follows:

$$F = -TS_{\text{poly}} - TS_{\text{mix}} + E_{\text{vdW}} + F_{\text{acid-base}}^{\text{mix}} + E_{\text{electro}} + E_{\text{rep}}$$
(1)

Here, the first two terms in eq 1 describe the conformational entropy of the polyelectrolyte chains and the mixing (or translational) entropy of the solvent (water) and mobile ions. The next contribution $E_{\rm vdW}$ stems from the nonsteric van der Waals effective energy between polymer beads. The next two terms are related to the free energy associated with the acid—base chemical equilibrium and the electrostatic interaction. The term $E_{\rm rep}$ represents the steric repulsion between all species. Next, we discuss each of the contributions in more detail

The conformational entropy of the polymer is given by

$$-\frac{S_{\text{poly}}}{k_{\text{B}}} = \int \sigma_{\text{g}}(\mathbf{r}(\mathbf{s})) \sum_{\alpha} P(\mathbf{r}(\mathbf{s}), \alpha) \ln(P(\mathbf{r}(\mathbf{s}), \alpha)) d\mathbf{s}$$
(2)

where s is a parametrization of the membrane interface area that is tethered with chains. ds is the area element, and the integral runs over the area where the polymers are anchored. $\sigma_{\rm g}({\bf r})$ is the grafting density of chains at ${\bf r}$, and $P({\bf r},\alpha)$ denotes the probability of finding a polyelectrolyte chain anchored at ${\bf r}$ in a certain conformation α . In principle, the sum includes all possible polyelectrolyte conformations. In practice, we generate a large unbiased set of polymer confirmation using the rotational isometric state model (RIS). We only consider those conformations that are self-avoiding and do not overlap with the walls of the nanopore.

Next, the mixing or translational entropy of all mobile species is given by

$$-\frac{S_{\text{mix}}}{k_{\text{B}}} = \sum_{i} \int \rho_{i}(\mathbf{r}) [\ln(\rho_{i}(\mathbf{r})\nu_{\text{w}} - 1] d\mathbf{r}$$
(3)

where $\rho_i(\mathbf{r})$ is the number density of the species i and index i runs over all the molecular species, which are water, Na⁺, Cl⁻, H⁺, and OH⁻.

The term $E_{\rm vdW}$ represents the effective van der Waals interactions between all polymer segments and accounts for the solvent quality. It is represented as follows:

$$-E_{\text{vdW}} = \iint \frac{\chi g(|\mathbf{r} - \mathbf{r}'|)}{2} \langle \rho_{\text{p}}(\mathbf{r}) \rangle \langle \rho_{\text{p}}(\mathbf{r}') \rangle \, d\mathbf{r} \, d\mathbf{r}'$$
(4)

Here, χ is the strength of the attractive interactions between the polymer segments, $g(|\mathbf{r}-\mathbf{r}'|)$ accounts for the distance dependence of the interaction, 26 and $\langle \rho_{\rm p}(\mathbf{r}) \rangle$ is the average density of polymer segments at position \mathbf{r} . $\langle \rho_{\rm p}(\mathbf{r}) \rangle$ is determined by the probability of the chain conformations, $P(\mathbf{r},\alpha)$, through the following expression: $\langle \rho_{\rm p}(\mathbf{r}) \rangle = \int \mathrm{d}\mathbf{s}' \sum_{a} \sigma_{\rm g}(\mathbf{r}'(\mathbf{s}')) P(\mathbf{r}'(\mathbf{s}'),\alpha) n_{\rm p}(\mathbf{r}'(\mathbf{s}'),\alpha,\mathbf{r})$, in which $n_{\rm p}(\mathbf{r}'(\mathbf{s}'),\alpha,\mathbf{r})$ dr is the number of monomers that a chain grafted at $\mathbf{r}'(\mathbf{s}')$ has in the volume element between \mathbf{r} and $\mathbf{r}+\mathrm{d}\mathbf{r}$ when it is in conformation α . The area element is denoted by ds', and the integral runs over the region where the polyelectrolytes are anchored. The effective van der Waals attractive strength is equal to 0 $k_{\rm B}T$ and 1 $k_{\rm B}T$. The former corresponds to the good solvent condition, and the latter equals the marginal poor solvent condition.

For a single basic molecule B in an aqueous environment, the acid—base reaction can be written as

$$BH^+ \rightleftharpoons B + H^+ \tag{5}$$

and the free energy contribution arising from this acid-base equilibrium is

$$\frac{F_{\text{acid-base}}}{k_{\text{B}}T} = \int \langle \rho_{p}(\mathbf{r}) \rangle [f(\mathbf{r}) \ln(f(\mathbf{r})) + (1 - f(\mathbf{r})) \ln(1 - f(\mathbf{r}))] d\mathbf{r}
+ \int \langle \rho_{p}(\mathbf{r}) \rangle [f(\mathbf{r}) \beta \mu_{\text{BH}^{+}}^{0} + (1 - f(\mathbf{r})) \beta \mu_{\text{B}}^{0}] d\mathbf{r}$$
(6)

Here, $f(\mathbf{r})$ denotes the fraction of basic monomers that is charged. The first and second integrals represent the mixing entropy of the charged and uncharged groups, while the remaining integral corresponds to the internal free energy of the charged and uncharged state of the monomers, with $\mu_{\mathrm{BH}^+}^0$ and μ_{B}^0 being their respective standard chemical potentials.

Next, the electrostatic contribution to the free energy functional is given by

$$F_{\text{electro}} = \int dV_{\text{mem}} \left(\langle \rho_q(\mathbf{r}) \rangle \psi(\mathbf{r}) - \frac{1}{2} \varepsilon_0 \varepsilon_{\text{mem}} (\nabla \psi(\mathbf{r}))^2 \right)$$

$$+ \int dV_{\text{s}} \left(\langle \rho_q(\mathbf{r}) \rangle \psi(\mathbf{r}) - \frac{1}{2} \varepsilon_0 \varepsilon_{\text{s}} (\nabla \psi(\mathbf{r}))^2 \right)$$

$$+ \int dS \sigma_q(S) \psi(S)$$
(7)

where $\varepsilon_{\rm mem}$ and $\varepsilon_{\rm s}$ correspond to the relative dielectric constant of the pore membrane and solvent, respectively. The variable $\psi({\bf r})$ represents the electrostatic potential, $\langle \rho_q({\bf r}) \rangle$ is the average charge density at position ${\bf r}$, and σ_q is the surface charge density. Inside the membrane, the charge density is assumed to be zero, i.e., $\langle \rho_q({\bf r}) \rangle = 0 \ \forall \ {\bf r} \in V_{\rm mem}$ while the charge density in the aqueous solution is given by $\langle \rho_q({\bf r}) \rangle = \sum_{i={\rm Na}^+,{\rm Cl}^-,{\rm H}^+,{\rm OH}^-} \rho_i({\bf r}) q_i + \langle \rho_q({\bf r}) \rangle f({\bf r}) q_p$, where the sum in the first term runs over all charged mobile species with q_i being the charge of species i ($i={\rm Na}^+,{\rm Cl}^-,{\rm H}^+,{\rm OH}^-$). The charge density stemming from the charged basic monomers is represented by the second term. In our system, the surface of the nanopore is assumed to have no free surface charges, which means $\sigma_q=0$. It only carries an induced polarization or bound charge density $\sigma_{\rm b}$. Variation of the electrostatic energy functional with respect to the electrostatic potential, $\psi({\bf r})$, yields

$$\nabla(\varepsilon_0 \varepsilon_{\text{mem}} \nabla \psi(\mathbf{r})) = -\langle \rho_q(\mathbf{r}) \rangle \ \forall \ \mathbf{r} \in V_{\text{mem}}$$

$$\nabla(\varepsilon_0 \varepsilon_s \nabla \psi(\mathbf{r})) = -\langle \rho_q(\mathbf{r}) \rangle \ \forall \ \mathbf{r} \in V_s$$
(8)

The electrostatic boundary conditions for the interface between the pore surface and solvent are also given by functional variation:

$$-(\varepsilon_{\text{mem}} \vec{\nabla} \psi(\mathbf{r})|_{\partial V_{\text{mem}}} \cdot \hat{n} - \varepsilon_{\text{s}} \vec{\nabla} \psi(\mathbf{r})|_{\partial V_{\text{s}}} \cdot \hat{n}) = \sigma_{q}$$
(9)

Here \hat{n} is the normal vector of the interface that points from the solution side to the membrane side of the interface. Observe that we employ cylindrical coordinates (r, z, θ) to exploit the symmetry of the nanopore system. To improve computational efficiency, we assume azimuthal homogeneity, which means that all-position-related quantities change exclusively in the radial and axial directions. Therefore, for r=0 (along the pore axis), the electrostatic potential obeys the following symmetry condition:

$$\frac{\partial \psi(r,z)}{\partial r}\bigg|_{r=0} = 0 \tag{10}$$

Finally, the boundary condition at the reservoir edges follows the no flux boundary condition:

$$\vec{\nabla}\psi(\mathbf{r})\cdot\hat{n}=0\tag{11}$$

Here \hat{n} is the normal vector of the *z*-plane that separates the nanopore system from the reservoir.

It is important to emphasize that eq 8 is the mean-field equivalent of the Poisson equation for electrostatics since the electrostatic potential and the charge number density correspond to the ensemble averages. It can be considered as a generalized Poisson-Boltzmann equation. Notably, here, the thermodynamic averaged charge density of the ions and polyelectrolyte results from the free energy minimization and therefore contains the molecular details of the system, which include, among others, the inter- and intrachain correlations of the polyelectrolyte chain. It is important to realize that for a neutral noncharged polymer system, under good solvent conditions, our theory includes intrachain correlations exactly since we explicitly include chain conformations. On the other hand, interchain interaction is treated in a mean-field level. Similarly, electrostatic interactions are only considered at the level of the average charge density, and as such, electrostatic interactions do not contain intrachain correlation directly but only implicitly via the chain conformation. As a result, the theory goes well beyond the traditional Poisson-Boltzmann approximation. Notice also that we solve this generalized Poisson equation for both the aqueous solution region and the membrane region. Previously, it had been assumed $\varepsilon_{\text{mem}} = 0$, and hence we did not need to solve for the Poisson equation inside of the membrane.

The last term in the free energy, $E_{\rm rep}$, describes the excluded volume interactions between all molecules, which are considered by assuming that the system is incompressible at every position:

$$\sum_{i=w,\mathrm{Na}^+,\mathrm{Cl}^-,\mathrm{H}^+,\mathrm{OH}^-} \rho_i(\mathbf{r})\nu_i + \langle \rho_{\mathrm{p}}(\mathbf{r}) \rangle \nu_{\mathrm{p}} = 1$$
(12)

Here v_i is the volume of mobile species i and v_p is the volume of the polymer segment.

Minimization of the free energy results in explicit expressions for the system variables $\rho_i(\mathbf{r})$, $P(\mathbf{r},\alpha)$, and $f(\mathbf{r})$, which are listed in the Supporting Information. The unknowns that need to be determined are the lateral pressures, $\pi(\mathbf{r})$, and the electrostatic potentials, $\psi(\mathbf{r})$. To solve the molecular theory, the equations for the system variables, such as the densities, are substituted into the incompressibility constraint (eq 12) and the generalized Poisson-Boltzmann equation (eq 8), resulting in a set of integro-differential equations. To solve this problem numerically, we discretize the space to convert the differential equations describing the system into a set of coupled nonlinear equations, which we can then solve selfconsistently⁵⁸ for those unknowns. For brevity, we have discussed here only the important details of molecular theory. More information about the description of the free energy expression and minimization as well as numerical implementation can be found in the Supporting Information and our previous publications. 59

RESULTS AND DISCUSSION

Dielectric Effect on Charge Regulation Process. First, the charging behavior of polyelectrolytes end-tethered to the nanopore membrane with different dielectric constants is reviewed. To characterize the charging of weak polyelectrolytes, it is convenient to introduce the average degree of protonation of the basic groups, which is given by

$$\langle f_{\rm BH^{+}} \rangle = \frac{\int d\mathbf{r} f_{\rm BH^{+}}(\mathbf{r}) \langle \rho_{\rm B}(\mathbf{r}) \rangle}{\int d\mathbf{r} \langle \rho_{\rm B}(\mathbf{r}) \rangle}$$
(13)

Figure 2 presents the average degree of charge as a function of pH in three different dielectric constant regimes: (i) low $\varepsilon_{\rm mem}$

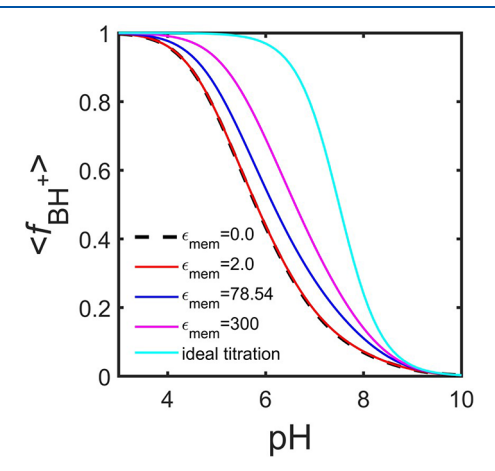


Figure 2. pH dependence of the average fraction of charged basic monomers in weak polybases that are end-tethered to the inner surface of the nanopore. The lines correspond membranes with different dielectric constants. From bottom to top the lines correspond to $\varepsilon_{\rm mem}=0$, 2, 78.54, and 300, respectively. The top line (cyan colored) represents the degree of protonation of the monomers in the bulk dilute solution. In this calculation, the pore radius and length are chosen as R=4 nm and L=10 nm. The chains in the polyelectrolyte-modified pore have chain length N=10 and grafting density $\sigma_{\rm g}=0.030$ nm⁻². Good solvent conditions are assumed. (The strength of the interaction between monomers is $\chi=0$ $k_{\rm B}T$.) The bulk salt concentration is equal to 1 mM.

regime, where $\varepsilon_{\rm mem} < \varepsilon_{\rm s}$; (ii) intermediate $\varepsilon_{\rm mem}$ regime, where $\varepsilon_{\rm mem} = \varepsilon_{\rm s}$; and (iii) high $\varepsilon_{\rm mem}$ regime, where $\varepsilon_{\rm mem} > \varepsilon_{\rm s}$. The bulk salt concentration is 1 mM. As we can see in Figure 2, the degree of charging of the polyelectrolytes in a nanopore is uniformly decreased as compared to the average protonation fraction of a single isolated monomer in dilute solution regardless of the value of $\varepsilon_{\mathrm{mem}}$. For comparison, the top line labeled "ideal titration" shows the degree of charge of the isolated base monomer in ideal solution, which, assuming ideal solution chemical equilibrium, corresponds to $f_{\rm BH}^+ = 1/(1 +$ $10^{(pH-pK_a)}$). The observed "titration" behavior can be explained as follows. For low pH values protonation of a single isolated monomer would be favored, but then the concentration of charged monomers within a confined nanopore would be considerable. This would result in strong electrostatic repulsions. The system employs several mechanisms to counteract these unfavorable electrostatic repulsions. A process known as charge regulation is one of those responses that can mitigate electrostatic repulsions. It involves shifting the acidbase equilibrium toward its uncharged state to reduce the net charge of the confined polymers. This reduces electrostatic

repulsions, but simultaneously, chemical work needs to be performed to shift the acid-base chemical equilibrium. Two other mechanisms that reduce unfavorable electrostatic repulsions are counterion confinement and chain stretching. Namely, the system can introduce additional counterions into the brush, hence increasing electrostatic screening. A loss of translational entropy of the counterions occurs as a result of counterion confinement. Moreover, the polymer chains can stretch to reduce electrostatic repulsions within the chain. However, chain stretching will cause a decrease in the conformational entropy of chains and cannot negate electrostatic repulsions between neighboring charged segments along the chain. Although all these processes are entropically unfavorable, they are compensated by a reduction in electrostatic repulsions. Thus, the fraction of protonated monomers and the structure of the polymer layer inside the nanopore result from a delicate balance and interplay between the different opposing chemical and physical interactions, which include the conformational entropy of the polymers, the translational entropy of the ions, and electrostatic interactions.

A significant finding, apparent from Figure 2, is that there is a considerable difference in the degree of dissociation of the basic monomers for the three permittivity regimes. For example, at pH = 6 we predict $\langle f_{\rm BH}^+ \rangle$ = 0.55 for $\varepsilon_{\rm mem}$ = 78.54 and find that the average degree of charge increases by more than ~25% to $\langle f_{\rm BH}^+ \rangle = 0.69$ for a membrane with a relative dielectric constant of $\varepsilon_{\rm mem}$ = 300. On the other hand, for a membrane with $\varepsilon_{\rm mem}$ = 2, we find that the average degree of charge reduces to $\langle f_{\rm BH^+} \rangle = 0.44$, more than 25% reduction. Consequently, there is almost a 50% change in the average degree of charging. Observe that the "titration" curve for a membrane with a dielectric constant of $\varepsilon_{\rm mem}$ = 0 is very similar and almost identical with that of a membrane with a permittivity of ε_{mem} = 2 because the difference in membrane permittivity is very small. Therefore, the past approximation of assuming $\varepsilon_{\mathrm{mem}}$ = 0 for low-permittivity membranes is valid. In general, if the charging behavior of a membrane case $\varepsilon_{\mathrm{mem}} = \varepsilon_{\mathrm{s}}$ is chosen as a reference state, we observe that, relative to this state, the degree of charge regulation is suppressed when the membrane has a high dielectric constant, whereas the opposite trend happens in the presence of a low-permittivity substrate. This phenomenon can also be clearly observed from the local degree of protonation shown in Figure 3D-F (for pH = 6). Not only does the local degree of protonation change significantly as a function of dielectric constant, but also, for example, the charge distribution profiles inside the nanopore with different ε_{mem} presented in Figure 3G–I (for pH = 6) demonstrate a permittivity-induced change in polyelectrolyte charges. It is clearly observable that increasing $\varepsilon_{\mathrm{mem}}$ causes a substantial rise in polyelectrolyte charges. More specifically, the maximum polymer charge density rises from 0.11 to 0.26 e/ nm³ when ε_{mem} is changed from 2 to 300.

To explain the occurrence of these differences, as well as to understand how the dielectric surface properties impact the charging behavior of weak polyelectrolytes, it is instructive to consider the shape and the size of electrostatic potential, because the strength of the electrostatic interactions determines the amount of charge regulation. First, an induced surface polarization charge density, $\sigma_{\rm b}$, occurs as a result of the permittivity difference at the solvent—membrane interface. It can be calculated as follows:

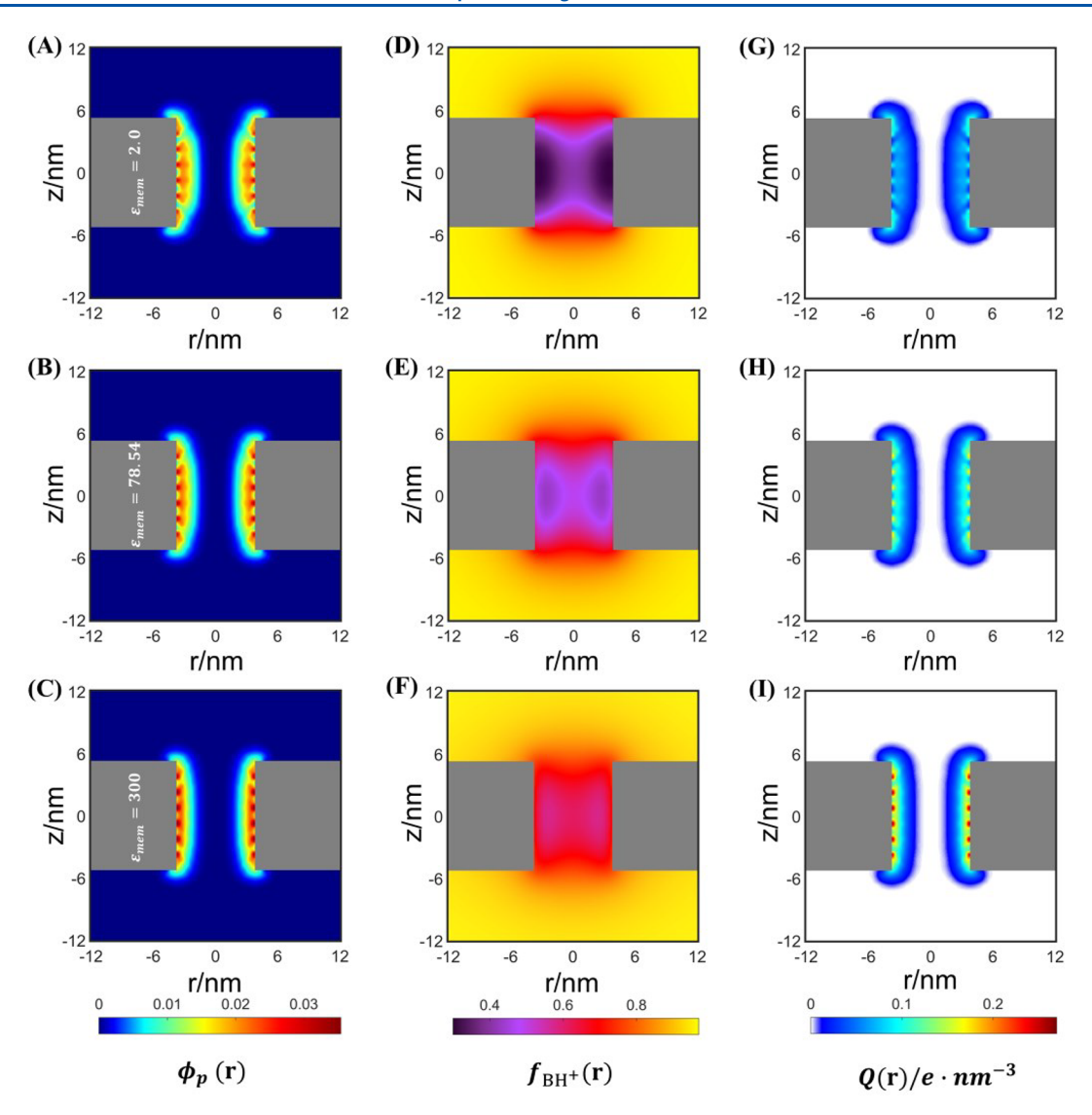


Figure 3. Color maps of the (A–C) polymer volume fraction, (D–F) fraction of charged basic monomers, and (G–I) charge distribution inside the nanopore with ε_{mem} = 2 (top), ε_{mem} = 78.54 (middle), and ε_{mem} = 300 (bottom). The bulk pH is chosen as 6. Other calculation parameters are the same as in Figure 2.

$$\vec{\mathbf{P}}_i = \varepsilon_0 (\varepsilon_i - 1) \vec{\mathbf{E}}_i$$

$$\sigma_b = (\vec{\mathbf{P}}_s - \vec{\mathbf{P}}_{mem}) \hat{\mathbf{n}}$$
(14)

Here \vec{P}_s and \vec{P}_{mem} are induced polarization at the solution and membrane side of the interface, respectively, and $\hat{\boldsymbol{n}}$ is the unit normal vector that points from the solution to the membrane side of the interface. The magnitude and sign of the bound (or polarization) surface charges are determined by the dielectric mismatch. As shown in Figure 4, the low dielectric wall has a positive polarization surface charge density, while the high dielectric one has a negative polarization surface charge density. For $\varepsilon_{\mathrm{mem}} = \varepsilon_{\mathrm{s}}$, there is no dielectric mismatch, and the bound surface charge density is zero. For a low-dielectric surface ($\varepsilon_{\rm mem} < \varepsilon_{\rm s}$), the positive surface polarization charge density results in an additional electrostatic repulsion between the surface and the positively charged monomers, which is mitigated by shifting the acid-base equilibrium toward the neutral, uncharged state further. Thus, the fraction of charged monomers drops as compared to the case where the surface and solvent do not have a dielectric mismatch, i.e., $\varepsilon_{\text{mem}} = \varepsilon_{\text{s}}$.

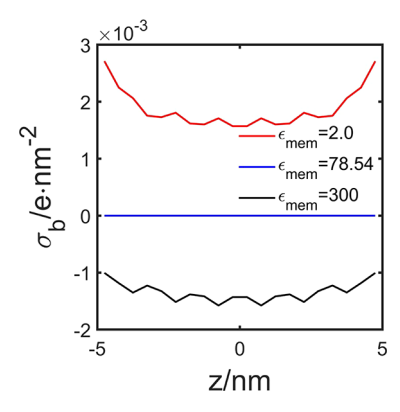


Figure 4. Surface polarization charge density profiles along the axial position of nanopore membrane. The density profile is observed for the nanopores formed in the membrane with $\varepsilon_{\rm mem}=2$ (red), $\varepsilon_{\rm mem}=78.54$ (blue), and $\varepsilon_{\rm mem}=300$ (black). The bulk pH is chosen as 6. Other calculation parameters are the same as in Figure 2.

Simultaneously, the polymers adopt more extended conformations, i.e., stretch, in an effort to negate the additional

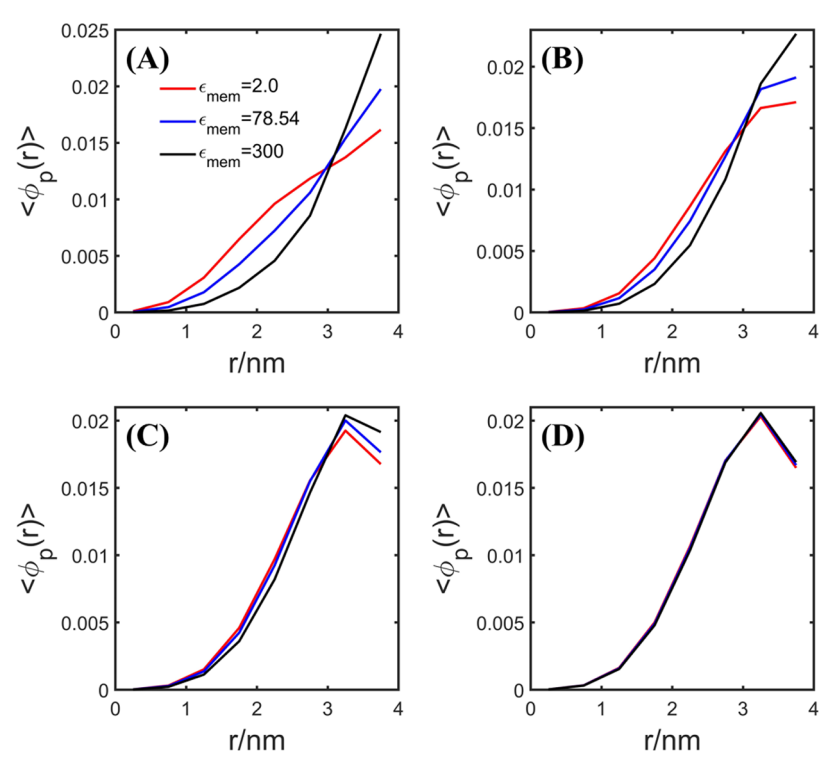


Figure 5. Radial profiles of polymer volume fraction within the nanopore in the case of various membrane permittivities at (A) pH = 3, (B) pH = 6, (C) pH = 7, and (D) pH = 8. Here, $\langle \phi_p(r) \rangle$ is calculated by $\langle \phi_p(r) \rangle = 1/L \int_{-L/2}^{L/2} \phi_p(r,z) \, dz$ The red, blue, and black lines correspond to cases where the dielectric constant of the nanopore membrane equals to 2, 78.54, and 300, respectively. Other calculation parameters are the same as in Figure 2.

electrostatic repulsions between the positively induced surface charges and positively charged monomers. As can be observed from the polymer morphologies (Figure 3A-C) and the radial distribution of polymer segments (Figure 5A,B), the polymers are more elongated in the axial direction for a low-dielectric surface as compared to a surface with $\varepsilon_{\rm mem}$ = $\varepsilon_{\rm s}$. As another important mechanism to offset the electrostatic repulsions, negatively charged counterions will be localized within the nanopore and confined close to charged monomers and the surface charges to increase electrostatic screening, while coions are expelled from the nanopore. This is clearly visible in the radial and axial ion distribution profiles shown in Figure 6. The figure indicates that the expulsion of the co-ions from the interior of the nanopore causes the co-ion concentration to drop by more than an order of magnitude as compared to the reservoir concentration. Notice also in Figure 6 the sizable difference the co-ion and counterion distributions have inside the nanopore as a function of dielectric properties of the membrane.

For a high-dielectric surface ($\varepsilon_{\rm mem} > \varepsilon_{\rm s}$), the opposite behavior can be observed as compared to a low-dielectric surface. Namely, the negatively induced surface polarization charges cause an extra electrostatic attraction with the positively charged monomers. This results in a shift of the acid—base equilibrium toward the charged state, and the fraction of charged monomers increases as compared to the case $\varepsilon_{\rm mem} = \varepsilon_{\rm s}$. At the same time, the polymers adopt more compact conformations to bring the negative surface charges and the positively charged monomers closer together (see Figures 3A–C and 5A,B). Concomitantly with charge regulation and changes in the polymer conformation, negative counterions are confined by the charge brush. However,

because the surface is now negatively charged, positively charged ions accumulate near the surface rather than negative ones, and sodium ions, together with the positively charged monomers, act as counterions for the surface charges. This difference is noticeable in the increase of the sodium ion distribution close to the surface, as shown in Figure 6D. Overall, the permittivity-induced variations in polyelectrolyte charge, surface polarization charge, and ion distribution result in different electrostatic environments inside the nanopore, as demonstrated by color maps of electrostatic potential for varying ε_{mem} in Figure 7A-C. A maximum change of up to 46% in local electrostatic potential can be found when $\varepsilon_{\mathrm{mem}}$ is changed. This difference is particularly evident in the radial profile of electrostatic potential near the inner surface of the nanopore (Figure 8A). Observe, for example, that the surface electrostatic potential for a low dielectric membrane equals about 100 mV while the high-dielectric membrane has a muchreduced surface electrostatic potential of around 55 mV. Here, we can clearly distinguish three entirely different electrostatic environments, which are a result of the effect of the dielectric mismatch. Note also that the normal gradient of the electrostatic potential, i.e., the electric field, is discontinuous across the dielectric boundary as stipulated by the electrostatic boundary conditions (see eq 10 and Figure 8B).

The degree of protonation of tethered polybases is closely correlated to the local environment the monomers experience. As explained above, the charge and structure of the polybase layer, the electrostatic potential, ion distribution, and the size of the bound surface charge density are all coupled together. Thus, variations in the charging behavior of the polybases due to changes in the dielectric properties of the substrate can alternatively be understood by considering the ion distribu-

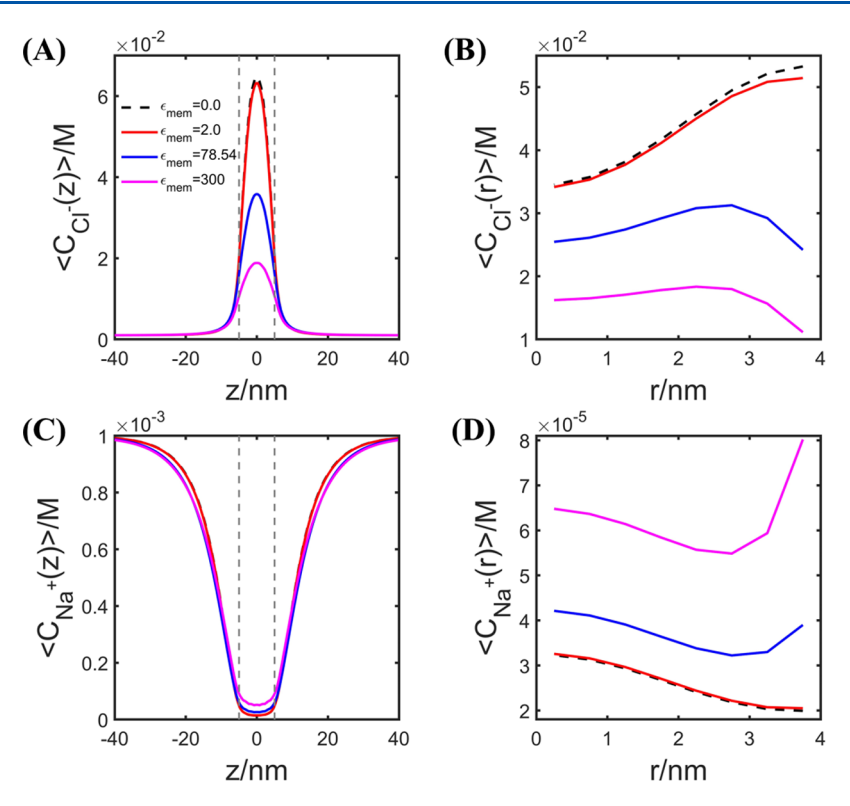


Figure 6. (A, C) Cross-sectional averaged anion and cation concentrations along the axis of the nanopore. Here, $\langle C_i(z) \rangle = 1/R^2 \int_0^R C_i(r,z)r \, dr$. The dashed lines mark out the location of the axial position of the two ends of the pore. (B, D) Concentration of salt ions inside the nanopore as a function of the distance to the center of the pore. $\langle C_i(r) \rangle = 1/L \int_{-L/2}^{L/2} C_i(r,z) \, dz$. The different color corresponds to different cases of membrane permittivity. For all cases, the bulk pH is chosen as 6, and other calculation parameters are the same as in Figure 2.

tions. Hence, it is instructive to study the distributions of the different charged components in the system as a function of the dielectric constant of the membrane as well. We illustrate this for pH = 6 (see Figures 6 and S1). The distributions of all mobile ions are affected by the dielectric characteristics of the pore membrane. When the pore wall has a low dielectric constant, $\varepsilon_{\mathrm{mem}} < \varepsilon_{\mathrm{s}}$, the positive surface polarization charges attract the negatively charged ions (Cl- and OH-) to the surface and, on the other hand, repel positively charged ions (Na+ and H+) and positively charged monomers from the surface. In contrast, the negative polarization of a highdielectric pore wall, $\varepsilon_{\rm mem} > \varepsilon_{\rm s}$, suppresses the concentration of negatively charged ions while enhancing that of positively charged ions within the pore. The local chemical balance of the basic monomers shifts toward the charged state when the local concentration of hydroxyl ions is lowered, and the equilibrium shifts in the opposite direction as it increases. Thus, the hydroxyl distribution offers a complementary explanation for the observation that the average protonation fraction is larger for $\varepsilon_{\rm mem} > \varepsilon_{\rm s}$ and lower for $\varepsilon_{\rm mem} < \varepsilon_{\rm s}$ compared to $\varepsilon_{\rm mem} = \varepsilon_{\rm s}$.

We have also investigated the effect of having polyacids instead of polybases, as illustrated in Figure S2. This "titration" curve, similar to Figure 2, shows the average charge fraction of polyacids end-tethered to the inner wall of nanopore as a function of pH. Identical dimensions and conditions are assumed for this system. We find similar qualitative charging behavior as a function of membrane permittivity for polyacids as compared to polybases. Obviously, the trends are reversed as a function of pH. Likewise, changing the solvent condition from $\chi = 0~k_{\rm B}T$ (good solvent) to $\chi = 1~k_{\rm B}T$ (marginal poor

solvent) showed similar trends in the dissociation behavior (see Figure S3). But the quantitative features, like the amount of charge and polymer and its distribution, are slightly different because reducing the solvent quality leads to an increased attraction among the monomers, which results in increased polymer density, causing a potential increase in the number of charges in the layer. In response, the system charge regulates and shifts the chemical equilibrium further to the neutral state. For instance, at pH = 7 the average charge fraction equals $\langle f_{\rm BH^+} \rangle = 0.210$ for good solvent but $\langle f_{\rm BH^+} \rangle = 0.207$ for marginal poor solvent conditions when $\varepsilon_{\rm mem} < \varepsilon_{\rm s}$. The differences are noticeable for higher pH. Because at higher pH values the number of charges, i.e., electrostatic interactions, decreases, the van der Waals interactions become more important. This difference also illustrates that the various physical and chemical interactions as well as the structural organization occurring within a polymer nanopore are all coupled together. We have not explored larger van der Waals attractions between the monomers because poor solvent conditions can lead to polymer collapse and phase separation within the polymer layer. 45,60 Here in this study, we focus on how the dielectric properties of the supporting membrane affect the delicate balance between physical and chemical interaction and structural organization of the polymer within the nanopore.

Dielectric Effect on Polymer Morphology. The discussion above demonstrates that the permittivity contrast between membrane and solution not only alters the ion distribution and charging behavior of the ionizable monomers but also affects the structure of the polyelectrolyte layer. Here, we examine in depth the pH dependency of the surface

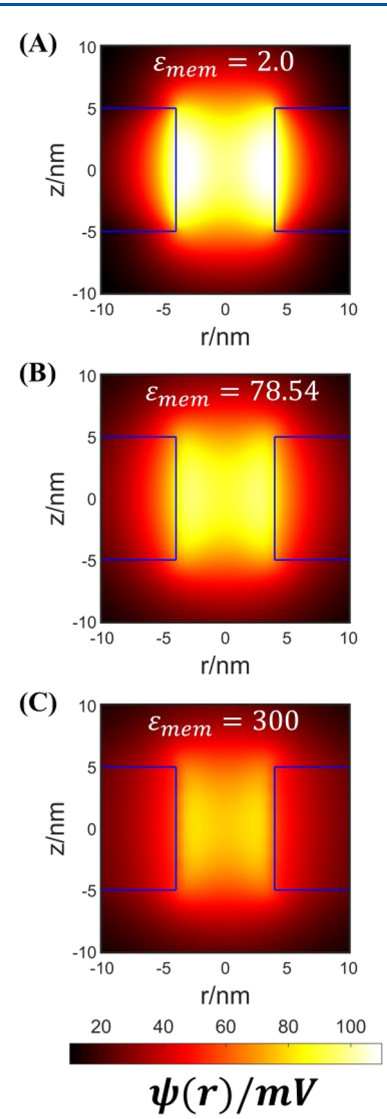


Figure 7. Color maps of electrostatic potential for the nanopore formed in the membrane with (A) $\varepsilon_{\rm mem}=2$, (B) $\varepsilon_{\rm mem}=78.54$, and (C) $\varepsilon_{\rm mem}=300$. The bulk pH is chosen as 6. Other calculation parameters are the same as in Figure 2.

dielectric on the polyelectrolyte structure and how this morphological change influences the nanoscale transport through the pore. In Figure 5A, we present the radial distribution of polymer chains inside the nanopore to illustrate the influence of membrane permittivity on brush structure at a relatively low pH condition. The basic monomers are nearly fully protonated at pH = 3, as illustrated in the "titration" curve of Figure 2. It is reasonable to expect that the dielectric constant of the pore membrane has only a minor impact on the charging behavior of the polyelectrolytes, which is confirmed by both Figure 2 and the local protonation degree in Figure S4D-F. Even though polymers have an almost identical degree of charge for all three dielectric conditions, we still observe that the polymer layer is structurally arranged differently for different membrane permittivities. For $\varepsilon_{\rm mem}$ = 2, the strong electrostatic repulsions between positive induced surface polarization charges and the likewise positively charged polymers cause the brush to expand. For $\varepsilon_{\rm mem}$ = 300, the negative surface polarization charges attract the charged polyelectrolyte monomers, which leads to contraction of the

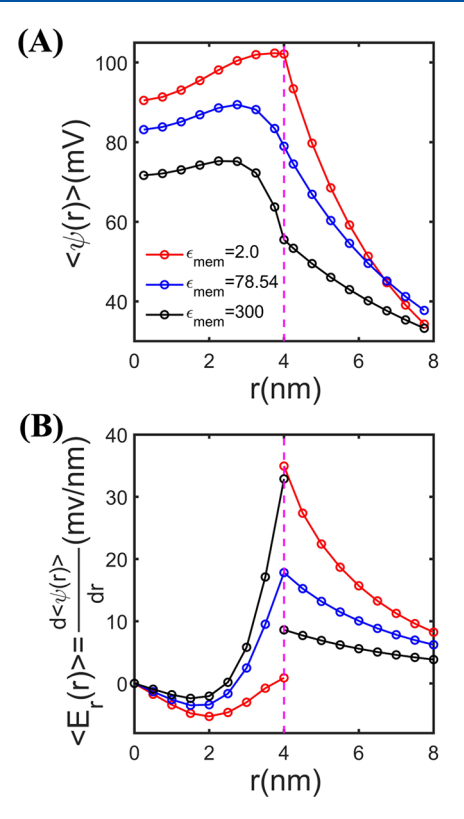


Figure 8. (A) Radial profile of the electrostatic potential near the inner surface of the nanopore membrane. $\langle \psi(r) \rangle$ can be calculated by $\langle \psi(r) \rangle = 1/L \int_{-L/2}^{L/2} \psi(r,z) \, \mathrm{d}z$. (B) Strength of the electric field in the radial direction, i.e., the derivative of the electrostatic potential with respect to the radial position, as a function of the distance r from the nanopore center. Vertical dashed line indicates the position of the membrane interface. It can be seen clearly that the derivative of the potential at the interface is discontinuous.

polymer layer. This structural transition is also validated by comparing the color maps of polymer volume fraction for different $\varepsilon_{\rm mem}$ regimes, which are plotted in Figure S4A–C. Noteworthy is the fact that this difference in polymer distribution within the nanopore can also result in a significantly distinct charge distribution, despite the similar charging behavior of the polyelectrolyte in the three dielectric substrates at pH = 3.0, as depicted in Figure S4G–I. Figure S4A–C also shows a feature of the polymer structures shared by all three $\varepsilon_{\rm mem}$ cases, namely that the polymers at the pore edges escape the nanopore at low pH, e.g., pH = 3. The reason for this behavior is that the segments tend to be expelled from the nanopore to maximize the conformational entropy of the chains while minimizing the strong electrostatic repulsions due to the high concentration of charged polymers inside the pore.

Increasing pH can lead to a drop in the degree of charge and the polymer structure changes accordingly. For example, the color maps of polymer volume fraction in Figure S5A–C show that the chains are collapsed into the nanopore at pH = 8. We have also plotted the polymer conformation at various pH values in a single diagram (see Figure S6) to demonstrate this pH-induced change in polymer morphology in greater detail. Next, we explore how dielectric effects influence the polymer structure at higher pH values. As illustrated in Figure 5B–D, the effect of the dielectric constant of the substrate on the polymer structure starts to diminish with increasing pH values. Taking pH = 8 as an example and comparing the polymer

distributions for the different cases of membrane permittivity, as shown in Figure S5A-C, reveal a large degree of similarity between the structural organization of the polymer layer. Thus, the results here further evidence the decreasing impact of the substrates' dielectric properties on the polymer structure as pH values are being raised. Increasing pH results in a considerable drop in the polymer charge, which causes the electrostatic interactions to weaken, and concomitantly, the surface polarization charge density is reduced. Consequently, the effect of dielectric mismatch on the polymer structure at high pH is only modest. Keep in mind, however, that in this pH range the dielectric property of the nanopore membrane still has a significant influence on the charging behavior of polyelectrolytes. For example, at pH = 8, $\langle f_{BH^{+}} \rangle$ = 0.07 for $\varepsilon_{\rm mem}$ = 2 and $\langle f_{\rm BH^+} \rangle$ = 0.14 for $\varepsilon_{\rm mem}$ = 300. Likewise, the local degree of charge and charge density, shown in Figure S5D-I, are different for distinct dielectric membranes. In summary, changing pH not only results in a qualitative change of the polymer structure but also determines the role of membrane permittivity in polymer structure.

The polymer structure inside the nanopore is closely related to the ability of the nanopore to transport or filter cargoes. To investigate how the structural changes in the polymer layer induced by the dielectric contrast can influence cargo translocation through the nanopore, the potential of mean force (PMF) is calculated for a cargo that solely interacts with the polymers and wall through steric repulsions. The PMF at position **r** equals the work required to transport the cargo from the bulk solution to **r**, which is expressed as follows:

$$\Delta F_{\text{PMF}} = F(\mathbf{r}_{\text{cargo}} = \mathbf{r}) - F(\mathbf{r}_{\text{cargo}} = \infty)$$
(15)

The particle will be unable to pass through the pore if it encounters a potential barrier that is several times greater than the thermal fluctuation. The transport test is performed at pH = 3. This value is chosen because a large effect of the substrate permittivity on the polyelectrolyte structure is observed for pH = 3. We limit the PMF calculation to medium cargo sizes compared to the nanopore radius because small cargoes, insensitive to the dielectric properties of the membrane, can diffuse easily through the nanopore, as demonstrated in Figure S7. On the other hand, in the case of large-sized cargo as compared to the nanopore radius, the steric repulsion experienced by the large-sized cargo is dominated by the large conformational entropy loss of the polymer layer and therefore obstructs cargo diffusion, irrespective of the membrane dielectric properties. Observe that the permittivity-induced changes in polymer structure can greatly affect the free energy barrier in this scenario. Thus, the transport efficiency of medium-sized cargoes having a radius of 1.5 and 2 nm through the nanopore with different membrane permittivity is investigated here. The PMFs for these two different-sized cargos through the nanopore along the central axis are shown in Figure 9A,B. Free energy barriers located within the nanopore are observed for both cargo sizes. The free energy barrier occurs because the polymer layers are stretched at pH = 3 and sterically hinder the translocation of cargo through the pore. We also find that for nanoparticles with a radius of 2 nm the barrier height of the PMF experiences a large decrease from 4.17 to 1.31 k_BT when the dielectric constant of the membrane changes from a low to a high value. The PMF likewise reduces from 1.77 to 0.57 $k_{\rm B}T$ for nanoparticles having a radius of 1.5 nm. This trend in free energy implies that a change in dielectric properties of the membrane can lead to a

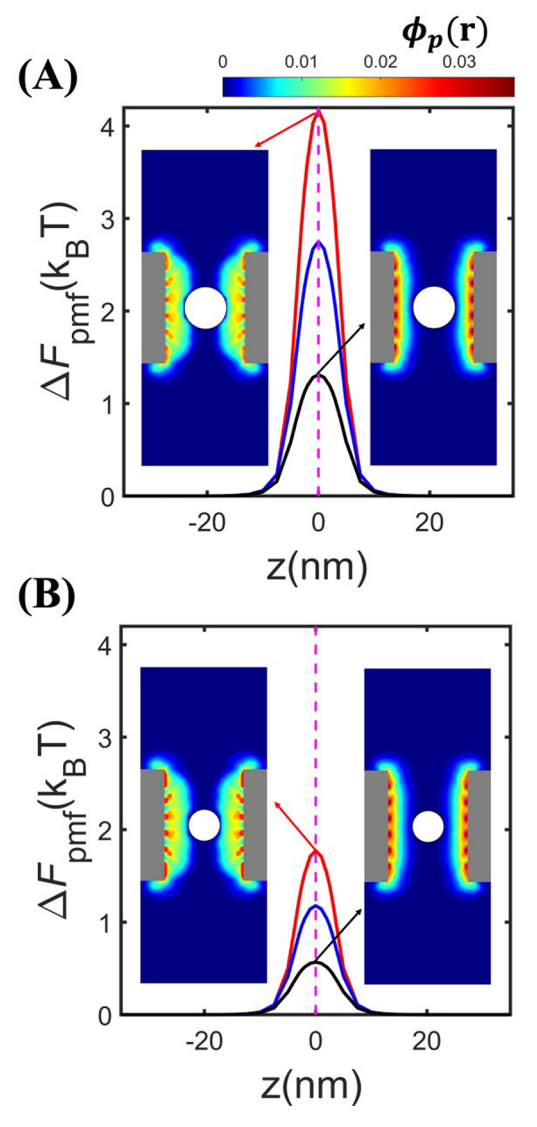


Figure 9. Potential of mean forces (PMFs) of the cargo with a radius of (A) 2 nm and (B) 1.5 nm through the nanopore formed in the membrane with different permittivity. The insets in the figure show color maps of the polymer volume fraction when the cargo is located at the axial center of the nanopore with $\varepsilon_{\rm mem}=2$ and $\varepsilon_{\rm mem}=300$. The bulk pH equals to 3. Other calculation parameters are the same as in Figure 2.

transition in cargo transport from blockage to successful passage through a nanopore. This behavior can be attributed to the fact that polyelectrolytes adopt less stretched conformations at larger $\varepsilon_{\rm mem}$. Furthermore, because the influence of dielectric mismatch on the brush structure is pH-dependent, one can easily control the permittivity-induced variation in cargo transport by tuning the pH. This can be seen in Figure S8, which shows that as the pH increases, the dielectric effect on the barrier height decreases. The findings in this section demonstrate that the dielectric membrane properties influence the molecular transport through the nanopore strongly, and thus the dielectric properties should be considered when designing novel nanopores for cargo translocation.

Effect of Salt Concentration. In the foregoing section, we demonstrated the dielectric effect on the charge regulation process of weak polyelectrolytes. Herein we investigate the impact of $\varepsilon_{\rm mem}$ on the brush charge and structure for different

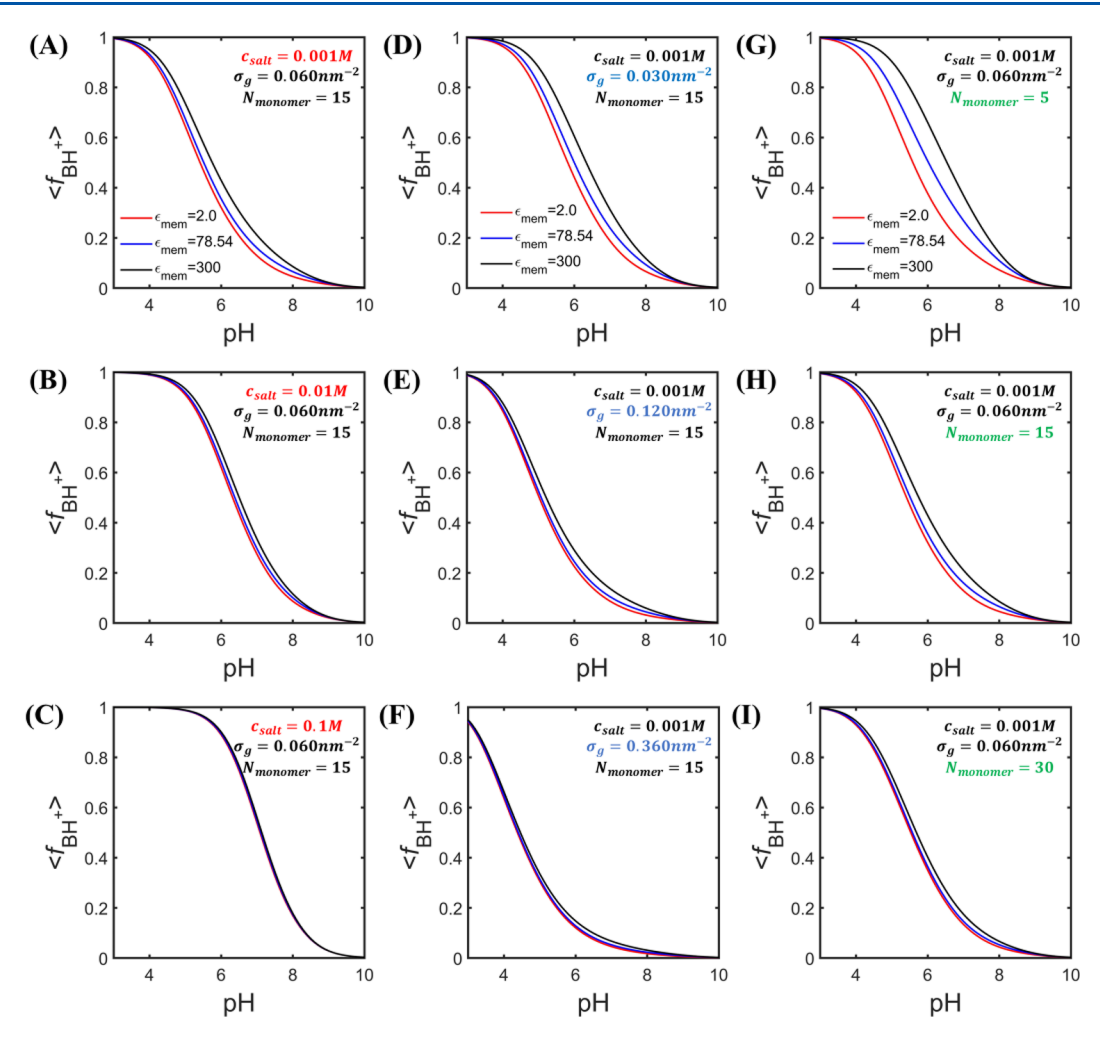


Figure 10. Variation of the protonation degree of basic monomers as a function of pH in the solid-state nanopore with different membrane permittivity. The permittivity-induced difference in charge regulation behavior has been observed in varying (A–C) salt conditions, (D–F) grafting densities, and (G–I) polymer length.

salt concentrations. In general, as the bulk salt concentration increases, the electrostatic interactions are screened, and accordingly, the effects of dielectric mismatch are expected to reduce since the size of the induced surface polarization density should decrease. To examine this in detail, the average protonation fraction of basic monomers for $\varepsilon_{\rm mem}$ = 2, 78.54, and 300 are compared under different salt conditions. The results are shown in Figure 10A-C. At low salt concentrations, a change in the value of membrane permittivity results in noticeable changes in the dissociation of monomers. More specifically, when ε_{mem} changes from 2 to 300, the average degree of protonation increases by 0.11 to 0.43 at pH = 6. Oppositely for high salt concentration, the dielectric effect has only a negligible effect on the polyelectrolyte charge because the screening effect dominates changes in the electrostatic interactions. For the results presented in Figure 10C, we find that the maximum increase in $\langle f_{\rm BH}^+ \rangle$ is only 0.01 at $c_{\rm salt} = 0.1$ M. The results clearly indicate that the effect of dielectric mismatch on the charging of confined weak polyelectrolytes is strongly dependent on the salt concentration. To explore in more depth the coupling between screening and dielectric mismatch, we present in Figure 11 the average degree of dissociation along the radial direction of the nanopore at varying salt conditions. Comparing the local degree of monomer dissociation for the nanopore systems with different

 $\varepsilon_{\rm mem}$ enables us to determine the strength and range of surface polarization effect. Regardless of salt concentration, the effect of dielectric mismatch is the strongest in the interfacial region. We also notice that the charging of the monomers away from the membrane becomes almost insensitive to the dielectric properties of the membrane when the salt concentration is relatively high. This stems from the fact that the electrostatic interactions between the surface polarization charges and all ions and charged monomers are gradually screened as more salts are added to the system. More importantly, the addition of salt causes a decrease in the surface polarization charge density (see Figure S9), which weakens the influence of surface polarization of the membrane even further.

Effect of Grafting Density and Polymer Length. In this section, we investigate how the grafting density and polymer molecular weight impact the dielectric effect on the charging behavior of the polyelectrolyte layer. The panels of the middle column of Figure 10, from top to bottom, show the degree of charge for rising grafting density (Figure 10D–F), while the panels of the right column pertain to increasing polymer length or molecular weight (Figure 10G–I), and the left column depicts the degree of protonation for increasing salt concentrations (Figure 10A–C). Clearly, the polymer grafting density, σ_g , is an important parameter that significantly influences the dissociation. Generally, with increasing grafting

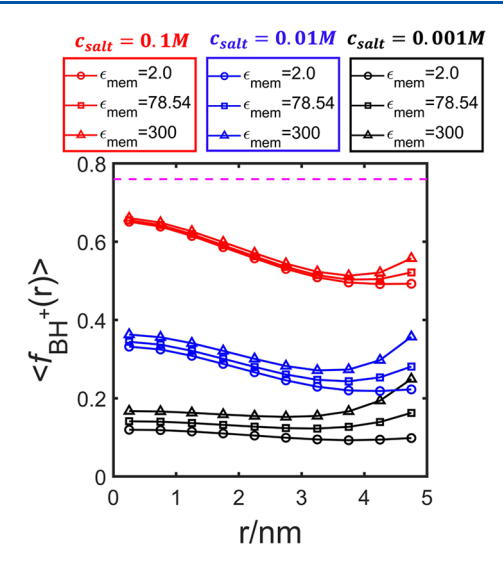


Figure 11. Variation of the degree of monomer dissociation as a function of the distance from the center of the pore. Different bulk concentrations are applied here: $c_{\rm salt}=0.1~{\rm M}~({\rm red}),~c_{\rm salt}=0.01~{\rm M}~({\rm blue}),$ and $c_{\rm salt}=0.001~{\rm M}~({\rm black}).~\langle f_{\rm BH}{}^{i}(r)\rangle = \int_{-L/2}^{L/2} f_{\rm BH}{}^{i}(r,z)\langle \rho_{\rm p}(r,z)\rangle$ dz. For each salt condition, the dissociation behavior of basic monomers is studied for three different dielectric constant regimes. The expected $\langle f_{\rm BH}{}^{i}\rangle$ from the bulk dilute solution is marked with a purple dashed line. Other calculation parameters: chain length, N=15; surface coverage, $\sigma_{\rm g}=0.060~{\rm nm}^{-2}$; good solvent conditions ($\chi=0~k_{\rm B}T$); pore radius, $R=5~{\rm nm}$; pore length, $L=10~{\rm nm}$; bulk pH, pH = 7.0.

density, the potential number of charged monomers grows. To avoid excess electrostatic repulsion, the fraction of charged monomers drops in weak polyelectrolyte layers. Figure 10D demonstrates that the degree of charge within the brush is closely correlated to the value of membrane permittivity in the regime of low grafting density. However, the effect of the membrane permittivity on the polyelectrolyte charging diminishes for higher grafting densities, as illustrated in Figure 10E,F. The maximum change of $\langle f_{\rm BH}^+ \rangle$ due to variations in the value of $\varepsilon_{\rm mem}$ significantly drops from 0.16 to 0.03 as $\sigma_{\rm g}$ increases from 0.03 to 0.36 nm⁻². To elucidate the origin of this observation, we compare the local variation of the averaged fraction of charged monomers along radial direction for different grafting densities in Figure S10. At lower grafting densities, the surface polarization has a greater impact on the charging regulation of monomers, and the influence is noticeable over greater distances. The influence of the membrane permittivity disappears away from the interfacial region at high grafting density. This bears qualitative similarity to the observed effect of salt concentration. This indicates that the effect of the membrane dielectrics is electrostatically screened. For a densely grafted and charged polymer layer, a large number of counterions will be confined in the nanopore. The confinement of a substantial amount of counterions inside the polymer layer causes the charged monomers to be electrostatically shielded from the interactions with surface polarization charges. Hence, the effects of having different dielectric surface properties diminish for denser layers. Oppositely for lower grafting densities, there is a noticeable influence.

As we previously noted, the magnitude of dielectric effects on monomer charging varies locally within the nanopore. The strongest effects are always found near the pore membrane. This observation suggests that the polymer length will also have a considerable impact on the extent of dielectric effects because the polymer length also determines the spatial distribution of the monomers. To examine this, the charging behavior of monomers in the nanopores with different $arepsilon_{\mathrm{mem}}$ are revisited, but this time we consider different polymer lengths. Figure 10G-I demonstrates that changing the dielectric properties of the membrane can significantly alter the dissociation of the monomers if short polymers are considered while grafting long polymers reduces the dielectric impact on the polyelectrolyte charge. The primary reason is that as the grafted polymers get longer, a considerable fraction of ionizable monomers are distributed away from the pore membrane, which is clearly evidenced by the radial distribution of monomers in Figure S11. Hence, they are electrostatically shielded from the electrostatic surface interactions and thereby from potential changes in those surface interactions caused by different membrane dielectric properties.

Our systematic study reveals that the dielectric effect on monomer dissociation can be amplified by choosing a low salt concentration, polymer grafting density, and short polymer length. When these three extreme conditions are satisfied simultaneously, the dielectric characteristics of the surface are a significant factor that affects the charging behavior of weak polyelectrolytes, as demonstrated in Figure S12, which shows the fraction of charge as a function of pH for these extreme conditions.

SUMMARY AND CONCLUDING REMARKS

In the present work, polyelectrolyte functionalized nanopores with different membrane properties are studied with a molecular theory. The theory explicitly considers the coupling between polymer conformations, chemical reactions, and the dielectric properties of the nanopore wall. Employing this state-of-the-art approach, we established a quantitative relationship between the charge and charge regulation process of the weak polyelectrolytes and the dielectric properties of the nanopore surface. The permittivity mismatch at the solventmembrane interface gives rise to a surface polarization charge, which causes a modulation of the charging behavior of polyelectrolytes. As compared to the membranes that have no dielectric contrast, the positively polarized membrane ($arepsilon_{
m mem}$ < $\varepsilon_{\rm s}$) significantly enhances the concentration of counterions inside the nanopore, thereby shifting the acid-base equilibrium toward the uncharged state to a greater extent. The opposite trend happens when $\varepsilon_{\rm mem} > \varepsilon_{\rm s}$. The influence of surface polarization on monomer dissociation of the polyelectrolyte grafted inside the nanopore can also be controlled by tuning the salt concentration, grafting density, and polymer length or molecular weight. In this work, we have not included the effect of surface curvature on the surface polarization effect in this work yet. When we narrow down the nanopore radius (i.e., increase the surface curvature), the polymers are more confined inside the pore and get closer to the surrounding membrane. As we discussed before, the polarization effect is more pronounced in the interfacial region. As a result, the influence of membrane permittivity on the charge regulation of weak polyelectrolytes gets stronger. On the other hand, while widening the nanopore, the monomers become further away from the opposing surface. Thus, the influence of opposing membrane on the charging behavior of polymers gradually fades, leading to a weaker influence of membrane permittivity on polymer charges. This phenomenon

is supported by a comparison of polyelectrolyte protonation behavior in nanopores of different radii, as depicted in Figure S13. It will be interesting to investigate the dielectric effect on the charge regulation inside the planar polymer brush since it is the limiting case of the radius of curvature going to infinity. The findings presented here already suggest that the membrane permittivity will have less impact on the charging behavior inside the planar polyelectrolyte brush compared with the pore with high surface curvature. Observe that changing the nanopore radius or curvature has a similar effect on the charging behavior of weak polyelectrolyte as changing the surface grafting density. In both cases, it is polymer density that controls the amount of charge regulation, i.e., the shift of the acid-base equilibriums. The effect of surface grafting density has been described here. Therefore, a detailed study into the effects of curvature and the dielectric effect on charges inside the planar brushes is reserved for a separate future study since the current work focuses on understanding the effect of dielectric surface properties in the context of nanopore systems.

For a high-permittivity nanopore wall, the electrostatic attraction between induced negative surface polarization charges and positive charges of the polymers attached to the inner wall of the nanopore can drive the polymers to adopt more compact configurations. As a result of this compaction, the free-energy barrier that a particle that is translocated through the nanopore must overcome to penetrate the nanopore will decrease. On the other hand, polymers grafted to a low-permittivity substrate of the nanopore adopt more extended configurations, which prevent the cargo from being transported through the pore. Our predictions highlight the importance of the dielectric properties of the nanopore surface in controlling transport through the nanopore, which is useful for future experimental design of synthetic nanopores for selective translocation.

The molecular theory presented here considers many important details, such as a molecular representation of polymer conformations, charge regulation, and electrostatic interaction. However, it remains a mean-field approach that does not include electrostatic fluctuations. Another limitation of the theoretical approach is that we did not consider the dielectric property of the polymers themselves. We assumed that the dielectric constant of the polymer layer inside the nanopore corresponded to that of the solvent. Past calculations⁶¹ of planar polyelectrolyte brushes using a local dielectric constant, taken to be the linear volume-weighted average of the dielectric constant of water and the polymer, showed this to be a reasonable approximation for the low and intermediate density of polymer layers studied here. Only in very dense systems does the local dielectric environment appear to have a significant impact on charge regulation.⁶² Moreover, we assumed linear polarizability of the aqueous medium, which is an empirical description of the dielectric properties of the system. However, the local dielectric constant is determined by the local polarization, which is coupled to the local electric field and the local density of polymer and solvent. The description of the dielectric properties of the aqueous polymer medium inside the nanopore could be further improved by considering a polarizable molecular model.⁶³

Our previous investigations²⁹ on nanochannels modified with weak polyelectrolytes have already shown a strong pH dependence of the nanochannel conductance. The concentration of major charge carriers inside the channel is

determined by the amount of charged end-tethered polyelectrolytes, which depends on the reservoir pH. The permittivity-induced change in the protonation state of polyelectrolyte discovered in the present work implies a potential influence of dielectric mismatch on the ionic conductivity of the pore. The development of a non-equilibrium steady-state molecular theory to study the ion transport properties inside the polyelectrolyte functionalized nanopore with different membrane permittivity will be covered in a future study. Furthermore, the strong correlation between nanopore conductance and polyelectrolyte charges provides a great opportunity for experimentalists to indirectly investigate the different charging regulation mechanisms of weak polyelectrolytes inside nanopores with different membrane permittivity through analyzing the ion transport behavior.

So far, we considered nanopores with purely dielectric substrates. However, the substrate can also be metallic, or the substrate interface can have a combination of dielectric, metallic, and or charge regulating properties. Notably, metals have been considered frequently as a substrate for nanopores. Metal and dielectric surfaces can also present charge-regulating moieties, either due to deliberate surface modification, to improve processability, or as impurities. These different nanopores can be considered within the current approach by appropriately modifying the free energy functional and resulting electrostatic boundary condition.

In summary, we presented a systematic study of how dielectric surface properties affect structural and transport properties of polymer functionalized nanopores. The dielectric properties of the nanopore substrates manifest themselves through surface polarization. The monomer dissociation and distribution as well as nanoscale transport through the nanopore are significantly influenced and coupled with the surface polarization. The influence of various system parameters such as salt concentration, grafting density, and polymer length on the surface polarization and the nanopore properties has been established. Our theoretical findings here shed light on the importance of the dielectric properties of the nanopore substrate, which aid the future development of smart nanopores.

ASSOCIATED CONTENT

Supporting Information

The Supporting Information is available free of charge at https://pubs.acs.org/doi/10.1021/acs.macromol.2c01391.

A detailed description of the theoretical methods and minimization of the free energy; additional analysis of the dielectric modulation on ion distribution and nanoscale transport; supporting data showing how salt concentration, polymer length, and polymer grafting density influence the charge regulation process of endtethered weak polyelectrolytes in the nanopore (PDF)

AUTHOR INFORMATION

Corresponding Author

Igal Szleifer — Department of Biomedical Engineering, Chemistry of Life Processes Institute, and Department of Chemistry, Northwestern University, Evanston, Illinois 60208, United States; orcid.org/0000-0002-8708-0335; Email: igalsz@northwestern.edu

Authors

- Shiyi Qin − Department of Biomedical Engineering and Chemistry of Life Processes Institute, Northwestern University, Evanston, Illinois 60208, United States; orcid.org/0000-0002-8811-914X
- Rikkert J. Nap Department of Biomedical Engineering and Chemistry of Life Processes Institute, Northwestern University, Evanston, Illinois 60208, United States; orcid.org/0000-0002-1809-0249
- Kai Huang Institute of Systems and Physical Biology, Shenzhen Bay Laboratory, Shenzhen 518107, China

Complete contact information is available at: https://pubs.acs.org/10.1021/acs.macromol.2c01391

Author Contributions

S.Q. and R.J.N. contributed equally. S.Q. and R.J.N. developed the theory. S.Q. performed the calculations. S.Q. and R.J.N. wrote the original draft and all authors reviewed and edited the manuscript.

Notes

The authors declare no competing financial interest.

ACKNOWLEDGMENTS

I.S. acknowledges support from the National Science Foundation under Grant CBET-1833214. K.H. acknowledges support from the Key Area Research and Development Program of Guangdong Province (2020B010135001) and the Shenzhen Bay Laboratory Open Fund Project (SZBL2021080601013). This research was supported in part through the computational resources and staff contributions provided for the Quest high performance computing facility at Northwestern University which is jointly supported by the Office of the Provost, the Office for Research, and Northwestern University Information Technology.

REFERENCES

- (1) Cohen Stuart, M. A.; Huck, W. T. S.; Genzer, J.; Müller, M.; Ober, C.; Stamm, M.; Sukhorukov, G. B.; Szleifer, I.; Tsukruk, V. V.; Urban, M.; Winnik, F.; Zauscher, S.; Luzinov, I.; Minko, S. Emerging Applications of Stimuli-Responsive Polymer Materials. *Nat. Mater.* **2010**, 9 (2), 101–113.
- (2) Tagliazucchi, M.; Szleifer, I. Stimuli-Responsive Polymers Grafted to Nanopores and Other Nano-Curved Surfaces: Structure, Chemical Equilibrium and Transport. *Soft Matter* **2012**, *8* (28), 7292.
- (3) Ma, S.; Zhang, X.; Yu, B.; Zhou, F. Brushing up Functional Materials. NPG Asia Mater. 2019, 11 (1), 24.
- (4) Li, D.; Xu, L.; Wang, J.; Gautrot, J. E. Responsive Polymer Brush Design and Emerging Applications for Nanotheranostics. *Adv. Healthc. Mater.* **2021**, *10* (5), 2000953.
- (5) Pincus, P. Colloid Stabilization with Grafted Polyelectrolytes. *Macromolecules* **1991**, 24 (10), 2912–2919.
- (6) Ueno, K.; Inaba, A.; Kondoh, M.; Watanabe, M. Colloidal Stability of Bare and Polymer-Grafted Silica Nanoparticles in Ionic Liquids. *Langmuir* **2008**, 24 (10), 5253–5259.
- (7) Fuller, M.; Köper, I. Polyelectrolyte-Coated Gold Nanoparticles: The Effect of Salt and Polyelectrolyte Concentration on Colloidal Stability. *Polymers.* **2018**, *10* (12), 1336.
- (8) Raviv, U.; Giasson, S.; Kampf, N.; Gohy, J.-F.; Jérôme, R.; Klein, J. Lubrication by Charged Polymers. *Nature* **2003**, 425 (6954), 163–165.
- (9) Zhulina, E. B.; Rubinstein, M. Lubrication by Polyelectrolyte Brushes. *Macromolecules* **2014**, *47* (16), 5825–5838.
- (10) Wright, R. A. E.; Wang, K.; Qu, J.; Zhao, B. Oil-Soluble Polymer Brush Grafted Nanoparticles as Effective Lubricant Additives

- for Friction and Wear Reduction. Angew. Chemie Int. Ed. 2016, 55 (30), 8656-8660.
- (11) Cao, L.; Kruk, M. Grafting of Polymer Brushes from Nanopore Surface via Atom Transfer Radical Polymerization with Activators Regenerated by Electron Transfer. *Polym. Chem.* **2010**, *1* (1), 97–101.
- (12) Hou, X.; Yang, F.; Li, L.; Song, Y.; Jiang, L.; Zhu, D. A Biomimetic Asymmetric Responsive Single Nanochannel. *J. Am. Chem. Soc.* **2010**, *132* (33), 11736–11742.
- (13) Liu, J.; Pham, P.; Haguet, V.; Sauter-Starace, F.; Leroy, L.; Roget, A.; Descamps, E.; Bouchet, A.; Buhot, A.; Mailley, P.; Livache, T. Polarization-Induced Local Pore-Wall Functionalization for Biosensing: From Micropore to Nanopore. *Anal. Chem.* **2012**, *84* (7), 3254–3261.
- (14) Srinivas, A. R. G.; Hilali, R.; Damavandi, M.; Malmstrom, J.; Barker, D.; Weatherall, E.; Willmott, G.; Travas-Sejdic, J. Polymer Brush Functionalization of Polyurethane Tunable Nanopores for Resistive Pulse Sensing. ACS Appl. Polym. Mater. 2021, 3 (1), 279–289
- (15) Ochs, M.; Mohammadi, R.; Vogel, N.; Andrieu-Brunsen, A. Wetting-Controlled Localized Placement of Surface Functionalities within Nanopores. *Small* **2020**, *16* (17), 1906463.
- (16) Yameen, B.; Ali, M.; Neumann, R.; Ensinger, W.; Knoll, W.; Azzaroni, O. Ionic Transport Through Single Solid-State Nanopores Controlled with Thermally Nanoactuated Macromolecular Gates. *Small* **2009**, *5* (11), 1287–1291.
- (17) Zhang, H.; Hou, X.; Zeng, L.; Yang, F.; Li, L.; Yan, D.; Tian, Y.; Jiang, L. Bioinspired Artificial Single Ion Pump. *J. Am. Chem. Soc.* **2013**, *135* (43), 16102–16110.
- (18) Zhou, Y.; Guo, W.; Cheng, J.; Liu, Y.; Li, J.; Jiang, L. High-Temperature Gating of Solid-State Nanopores with Thermo-Responsive Macromolecular Nanoactuators in Ionic Liquids. *Adv. Mater.* **2012**, 24 (7), 962–967.
- (19) Cheng, L.; Cao, D. Designing a Thermo-Switchable Channel for Nanofluidic Controllable Transportation. *ACS Nano* **2011**, *5* (2), 1102–1108.
- (20) de Groot, G. W.; Santonicola, M. G.; Sugihara, K.; Zambelli, T.; Reimhult, E.; Vörös, J.; Vancso, G. J. Switching Transport through Nanopores with PH-Responsive Polymer Brushes for Controlled Ion Permeability. *ACS Appl. Mater. Interfaces* **2013**, *5* (4), 1400–1407.
- (21) Emilsson, G.; Sakiyama, Y.; Malekian, B.; Xiong, K.; Adali-Kaya, Z.; Lim, R. Y. H.; Dahlin, A. B. Gating Protein Transport in Solid State Nanopores by Single Molecule Recognition. *ACS Cent. Sci.* **2018**, *4* (8), 1007–1014.
- (22) Yong, H.; Molcrette, B.; Sperling, M.; Montel, F.; Sommer, J.-U. Regulating the Translocation of DNA through Poly(N-Isopropylacrylamide)-Decorated Switchable Nanopores by Cononsolvency Effect. *Macromolecules* **2021**, *54* (9), 4432–4442.
- (23) Yameen, B.; Ali, M.; Neumann, R.; Ensinger, W.; Knoll, W.; Azzaroni, O. Synthetic Proton-Gated Ion Channels via Single Solid-State Nanochannels Modified with Responsive Polymer Brushes. *Nano Lett.* **2009**, *9* (7), 2788–2793.
- (24) Hou, X.; Liu, Y.; Dong, H.; Yang, F.; Li, L.; Jiang, L. A PH-Gating Ionic Transport Nanodevice: Asymmetric Chemical Modification of Single Nanochannels. *Adv. Mater.* **2010**, 22 (22), 2440–2443.
- (25) Zhang, H.; Hou, X.; Hou, J.; Zeng, L.; Tian, Y.; Li, L.; Jiang, L. Synthetic Asymmetric-Shaped Nanodevices with Symmetric PH-Gating Characteristics. *Adv. Funct. Mater.* **2015**, 25 (7), 1102–1110.
- (26) Huang, K.; Szleifer, I. Design of Multifunctional Nanogate in Response to Multiple External Stimuli Using Amphiphilic Diblock Copolymer. J. Am. Chem. Soc. 2017, 139 (18), 6422–6430.
- (27) Perez Sirkin, Y. A.; Szleifer, I.; Tagliazucchi, M. Voltage-Triggered Structural Switching of Polyelectrolyte-Modified Nanochannels. *Macromolecules* **2020**, *53* (7), 2616–2626.
- (28) Qin, S.; Huang, K.; Szleifer, I. Design of Multifunctional Nanopore Using Polyampholyte Brush with Composition Gradient. *ACS Nano* **2021**, *15*, 17678.

- (29) Tagliazucchi, M.; Azzaroni, O.; Szleifer, I. Responsive Polymers End-Tethered in Solid-State Nanochannels: When Nanoconfinement Really Matters. *J. Am. Chem. Soc.* **2010**, *132* (35), 12404–12411.
- (30) Gonzalez Solveyra, E.; Nap, R. J.; Huang, K.; Szleifer, I. Theoretical Modeling of Chemical Equilibrium in Weak Polyelectrolyte Layers on Curved Nanosystems. *Polymers.* **2020**, *12* (10), 2282.
- (31) Karawdeniya, B. I.; Bandara, Y. M. N. D. Y.; Nichols, J. W.; Chevalier, R. B.; Dwyer, J. R. Surveying Silicon Nitride Nanopores for Glycomics and Heparin Quality Assurance. *Nat. Commun.* **2018**, 9 (1), 3278.
- (32) Chou, Y.-C.; Masih Das, P.; Monos, D. S.; Drndić, M. Lifetime and Stability of Silicon Nitride Nanopores and Nanopore Arrays for Ionic Measurements. *ACS Nano* **2020**, *14* (6), 6715–6728.
- (33) Antila, H. S.; Luijten, E. Dielectric Modulation of Ion Transport near Interfaces. *Phys. Rev. Lett.* **2018**, *120* (13), 135501.
- (34) Wang, R.; Gilboa, T.; Song, J.; Huttner, D.; Grinstaff, M. W.; Meller, A. Single-Molecule Discrimination of Labeled DNAs and Polypeptides Using Photoluminescent-Free TiO2 Nanopores. ACS Nano 2018, 12 (11), 11648–11656.
- (35) Zhang, M.; Chen, T.; Liu, Y.; Zhang, J.; Sun, H.; Yang, J.; Zhu, J.; Liu, J.; Wu, Y. Plasmonic 3D Semiconductor—Metal Nanopore Arrays for Reliable Surface-Enhanced Raman Scattering Detection and In-Site Catalytic Reaction Monitoring. ACS Sens. 2018, 3 (11), 2446–2454.
- (36) Buyukdagli, S. Dielectric Manipulation of Polymer Translocation Dynamics in Engineered Membrane Nanopores. *Langmuir* **2022**, 38 (1), 122–131.
- (37) Boda, D.; Valiskó, M.; Eisenberg, B.; Nonner, W.; Henderson, D.; Gillespie, D. The Effect of Protein Dielectric Coefficient on the Ionic Selectivity of a Calcium Channel. *J. Chem. Phys.* **2006**, *125* (3), 034901.
- (38) Zhang, B.; Ai, Y.; Liu, J.; Joo, S. W.; Qian, S. Polarization Effect of a Dielectric Membrane on the Ionic Current Rectification in a Conical Nanopore. *J. Phys. Chem. C* **2011**, *115* (50), 24951–24959.
- (39) Yuan, J.; Antila, H. S.; Luijten, E. Dielectric Effects on Ion Transport in Polyelectrolyte Brushes. *ACS Macro Lett.* **2019**, 8 (2), 183–187.
- (40) Yuan, J.; Antila, H. S.; Luijten, E. Structure of Polyelectrolyte Brushes on Polarizable Substrates. *Macromolecules* **2020**, 53 (8), 2983–2990.
- (41) Nguyen, T. D.; Olvera de la Cruz, M. Manipulation of Confined Polyelectrolyte Conformations through Dielectric Mismatch. *ACS Nano* **2019**, *13* (8), 9298–9305.
- (42) Curk, T.; Luijten, E. Charge Regulation Effects in Nanoparticle Self-Assembly. *Phys. Rev. Lett.* **2021**, *126* (13), 138003.
- (43) Peleg, O.; Tagliazucchi, M.; Kröger, M.; Rabin, Y.; Szleifer, I. Morphology Control of Hairy Nanopores. *ACS Nano* **2011**, *5* (6), 4737–4747.
- (44) Tagliazucchi, M.; Olvera de la Cruz, M.; Szleifer, I. Self-Organization of Grafted Polyelectrolyte Layers via the Coupling of Chemical Equilibrium and Physical Interactions. *Proc. Natl. Acad. Sci. U. S. A.* **2010**, *107* (12), 5300–5305.
- (45) Prusty, D.; Nap, R. J.; Szleifer, I.; Olvera de la Cruz, M. Charge Regulation Mechanism in End-Tethered Weak Polyampholytes. *Soft Matter* **2020**, *16* (38), 8832–8847.
- (46) Tagliazucchi, M.; Calvo, E. J.; Szleifer, I. Molecular Theory of Chemically Modified Electrodes by Redox Polyelectrolytes under Equilibrium Conditions: Comparison with Experiment. *J. Phys. Chem.* C 2008, 112 (2), 458–471.
- (47) Gong, P.; Wu, T.; Genzer, J.; Szleifer, I. Behavior of Surface-Anchored Poly(Acrylic Acid) Brushes with Grafting Density Gradients on Solid Substrates: 2. Theory. *Macromolecules* **2007**, *40* (24), 8765–8773.
- (48) Wang, D.; Nap, R. J.; Lagzi, I.; Kowalczyk, B.; Han, S.; Grzybowski, B. A.; Szleifer, I. How and Why Nanoparticle's Curvature Regulates the Apparent p K_a of the Coating Ligands. *J. Am. Chem. Soc.* **2011**, 133 (7), 2192–2197.

- (49) Nap, R. J.; Szleifer, I. How to Optimize Binding of Coated Nanoparticles: Coupling of Physical Interactions, Molecular Organization and Chemical State. *Biomater. Sci.* 2013, 1 (8), 814.
- (50) Bessonov, A.; Takemoto, J. Y.; Simmel, F. C. Probing DNA-Lipid Membrane Interactions with a Lipopeptide Nanopore. *ACS Nano* **2012**, *6* (4), 3356–3363.
- (51) Schibel, A. E. P.; Edwards, T.; Kawano, R.; Lan, W.; White, H. S. Quartz Nanopore Membranes for Suspended Bilayer Ion Channel Recordings. *Anal. Chem.* **2010**, *82* (17), 7259–7266.
- (52) Gao, J.; Guo, W.; Geng, H.; Hou, X.; Shuai, Z.; Jiang, L. Layer-by-Layer Removal of Insulating Few-Layer Mica Flakes for Asymmetric Ultra-Thin Nanopore Fabrication. *Nano Res.* **2012**, 5 (2), 99–108.
- (53) Ying, Y.-L.; Li, Y.-J.; Mei, J.; Gao, R.; Hu, Y.-X.; Long, Y.-T.; Tian, H. Manipulating and Visualizing the Dynamic Aggregation-Induced Emission within a Confined Quartz Nanopore. *Nat. Commun.* **2018**, *9* (1), 3657.
- (54) Mojtabavi, M.; Vahidmohammadi, A.; Liang, W.; Beidaghi, M.; Wanunu, M. Single-Molecule Sensing Using Nanopores in Two-Dimensional Transition Metal Carbide (MXene) Membranes. *ACS Nano* **2019**, *13* (3), 3042–3053.
- (55) Tagliazucchi, M.; Peleg, O.; Kröger, M.; Rabin, Y.; Szleifer, I. Effect of Charge, Hydrophobicity, and Sequence of Nucleoporins on the Translocation of Model Particles through the Nuclear Pore Complex. *Proc. Natl. Acad. Sci. U. S. A.* **2013**, *110* (9), 3363–3368.
- (56) Huang, K.; Tagliazucchi, M.; Park, S. H.; Rabin, Y.; Szleifer, I. Nanocompartmentalization of the Nuclear Pore Lumen. *Biophys. J.* **2020**, *118* (1), 219–231.
- (57) Flory, P. Statistical Mechanics of Chain Molecules; Hanser Publishers: 1989.
- (58) Tagliazucchi, M.; Rabin, Y.; Szleifer, I. Ion Transport and Molecular Organization Are Coupled in Polyelectrolyte-Modified Nanopores. J. Am. Chem. Soc. 2011, 133 (44), 17753–17763.
- (59) Nap, R.; Gong, P.; Szleifer, I. Weak Polyelectrolytes Tethered to Surfaces: Effect of Geometry, Acid—Base Equilibrium and Electrical Permittivity. J. Polym. Sci., Part B: Polym. Phys. 2006, 44 (18), 2638–2662.
- (60) Tagliazucchi, M.; Olvera de la Cruz, M.; Szleifer, I. Self-Organization of Grafted Polyelectrolyte Layers via the Coupling of Chemical Equilibrium and Physical Interactions. *Proc. Natl. Acad. Sci. U. S. A.* **2010**, *107* (12), 5300–5305.
- (61) Nap, R. J.; Tagliazucchi, M.; Szleifer, I. Born Energy, Acid-Base Equilibrium, Structure and Interactions of End-Grafted Weak Polyelectrolyte Layers. *J. Chem. Phys.* **2014**, *140* (2), 024910.
- (62) Nap, R. J.; Qiao, B.; Palmer, L. C.; Stupp, S. I.; Olvera de la Cruz, M.; Szleifer, I. Acid-Base Equilibrium and Dielectric Environment Regulate Charge in Supramolecular Nanofibers. *Front. Chem.* **2022**, DOI: 10.3389/fchem.2022.852164.
- (63) Nakamura, I.; Shi, A.-C.; Wang, Z.-G. Ion Solvation in Liquid Mixtures: Effects of Solvent Reorganization. *Phys. Rev. Lett.* **2012**, *109* (25), 257802.
- (64) Zhao, H.; Wang, C.; Vellacheri, R.; Zhou, M.; Xu, Y.; Fu, Q.; Wu, M.; Grote, F.; Lei, Y. Self-Supported Metallic Nanopore Arrays with Highly Oriented Nanoporous Structures as Ideally Nanostructured Electrodes for Supercapacitor Applications. *Adv. Mater.* 2014, 26 (45), 7654–7659.
- (65) Freedman, K. J.; Otto, L. M.; Ivanov, A. P.; Barik, A.; Oh, S. H.; Edel, J. B. Nanopore Sensing at Ultra-Low Concentrations Using Single-Molecule Dielectrophoretic Trapping. *Nat. Commun.* **2016**, *7*, 1–9.
- (66) Kumar, S.; Wittenberg, N. J.; Oh, S. H. Nanopore-Induced Spontaneous Concentration for Optofluidic Sensing and Particle Assembly. *Anal. Chem.* **2013**, 85 (2), 971–977.